Near-equilibrium desorption of helium films

M. Weimer, R. M. Housley,* and D. L. Goodstein
California Institute of Technology, Pasadena, California 91125
(Received 23 March 1987)

The thermal desorption of helium films in the presence of their equilibrium vapor is studied experimentally for small but rapid departures from ambient temperature. The results are analyzed within the framework of a quasithermodynamic phenomenological model based on detailed balance. Under the usual experimental conditions, isothermal desorption at the temperature of the substrate is a general prediction of the model which seems to be substantiated. For realistic adsorption isotherms the time evolution of the net desorption flux nevertheless appears to be governed by a highly nonlinear equation. In such circumstances, a number of characteristic relaxation times may be identified. These time scales are distinct from, and in general unrelated to, the coverage-dependent mean lifetime of an atom on the surface. To characterize the overall nonlinear evolution towards steady state, a global time scale, defined in terms of both initial- and steady-state properties, is introduced to summarize the experimental data. Internal evidence suggests a criterion for judging when collisions among desorbed atoms are unimportant. When this condition is satisfied, data for near-equilibrium desorption agree well with the predictions of the model. Combining our results with earlier data at higher substrate temperatures and different ambient conditions, the overall picture is consistent with scaling properties implied by the theory. We show that the values of the parameters deduced from a Frenkel-Arrhenius parametrization of the global relaxation times, as well as a variety of other aspects of desorption kinetics, are actually consequences of the shape of the equilibrium adsorption isotherm.

I. INTRODUCTION

The kinetics of the adsorption and desorption of atoms and molecules on solid surfaces is an area of considerable scientific and technological interest. While many of the technologically significant problems concern complex chemisorption systems, the relative simplicity and weak interactions responsible for physisorption give rise to the hope that the kinetics of these systems might be understood in terms of such fundamental quantities as the dynamic gas-surface interaction potential. The expression of interest in physisorption kinetics from this point of view has been marked by the recent appearance of an entire book devoted to the subject.[1] At the same time, a renewed awareness of the power and utility of phenomenological, quasiequilibrium approaches, emphasizing detailed balance[2–4] and equilibrium thermodynamic considerations,[5,6] has been voiced in the literature.

Over the past several years in our laboratory, flash desorption techniques have been used to measure the desorption times of helium films, the sticking probability for low-energy helium atoms incident on our substrates, and to provide evidence that helium atoms can be directly evaporated by nonequilibrium phonons.[7–9] During that same period, a continuum thermodynamic description was developed that showed promise of being able to account for the measured desorption times and other related phenomena.[2,10] In this paper we present new experimental data on the dynamical evolution of a rapidly heated helium film together with an extended and detailed phenomenological analysis that allows a direct comparison between this theory and the experiments.

As we shall see, the comparison is very successful. Our conclusion will be that, with reasonable assumptions about both the sticking coefficient and the qualitative character of the equation of state, our observations point to essentially equilibriumlike behavior. Because of the phenomenological nature of the analysis, our results do not resolve any fundamental theoretical problems, but they do aid in sorting out the differences between what microscopic theories predict and what experiments often measure. Further, they serve to explain the origin of a number of otherwise puzzling features of these and prior experiments.

Microscopic theories of desorption generally attempt to predict the mean residence time of an isolated atom on a homogeneous surface at temperature T. This quantity is universally parametrized in the Frenkel-Arrhenius form,

$$\tau=\tau_0 e^{E/k_B T}, \tag{1}$$

where E is usually of the order of the binding energy of the atom to the surface, but where the prefactor τ_0 varies considerably from one theory to another. Intimately related to the question of desorption rates is the probability that an incident atom will stick to the surface.

We shall argue that when a physisorbed film is disturbed from equilibrium with its vapor, its evolution toward a new dynamic steady state can be described by a set of coupled ordinary differential equations that is generally rendered nonlinear by the nonlinearity of the ad-

sorption isotherms (amount adsorbed versus vapor pressure at each temperature) of the film, even if the sticking probability is assumed to be insensitive to changes in coverage. Consequently, the time dependence of the desorption is not a simple exponential, and there is no single time constant to be compared to Eq. (1). Nevertheless, it is possible to extract from the predictions of the model the characteristic time to reach steady state that an experimentalist might extract from comparable data. When this time, which we call $\tau_{\rm exp}$, is analyzed in the time-honored Arrhenius plot ($\log_{10}\tau_{\rm exp}$ vs T_s^{-1}, where T_s is the substrate temperature), the result, like the real experimental data, is a very good straight line over decades of $\tau_{\rm exp}$, thus seeming to justify the use of Eq. (1). Like the real data, however, the slope of the plot is less than the binding energy, and the prefactor has no obvious interpretation.

In order to obtain easily measurable signals, prior experiments in our laboratory depended on very large disturbances of the film from equilibrium. For a variety of reasons, that made the results difficult to compare even to the phenomenological model, much less to microscopic theories. In this paper we present data for much smaller disturbances, where many of the previous difficulties are sidestepped. In this limit, we find not only qualitative but also quantitative agreement with the model. The new data agree with the older data where they overlap. The new data are made possible in part by an improved system of signal recovery, averaging, and handling, which also leads to a more sophisticated quantitative analysis of the data and qualitative comparison with the model. We are able to understand not only the gross time dependence, but also many more subtle features having to do with initial and final conditions, and involving adsorption as well as desorption.

This paper is organized as follows: In Sec. II we review the recent history out of which this work grows. In Sec. III we present the new theoretical analysis, and in Sec. IV the new experiments. We conclude in Sec. V with a few comments about the present situation.

II. HISTORICAL BACKGROUND

A few years ago, Sinvani *et al.*[7] reported a new technique for studying the desorption of thin helium films. The experimental arrangement was similar to that described below in Sec. IV. When the adsorption substrate was heated rapidly from ambient temperature T_0 to final temperature T_s, they found that the helium film reached a new steady-state thickness in a time τ that could be described by Eq. (1) with temperature T_s, exponent $E \simeq -\frac{2}{3}\mu_0$, where μ_0 was the film chemical potential *before* heating, and $\tau_0 \simeq 10^{-9}$ sec. These results did not correspond with any of the then available microscopic theories[11–21] which focused, primarily, on calculating the mean lifetime of a single atom in an assembly of independent particles on the surface. In other words, none of these theories addressed the problem of determining the relaxation time for a strongly interacting film, perturbed from equilibrium by rapid heating, to reach a new steady state in the presence of its equilibrium vapor.

In an attempt to explain this and other related experiments, Weimer and Goodstein[5,10] presented a simple analysis based on thermodynamic quasiequilibrium ideas. The rate of change of the coverage $n(t)$, or number of adsorbed atoms per unit area, when the sticking coefficient σ is assumed to be independent of temperature and coverage, as well as direction and energy, is given by

$$\frac{dn}{dt} = \sigma(J_i - J_o) , \tag{2}$$

where J_i is the flux incident from the vapor and J_o the flux desorbing from the heated surface. Presuming the vapor to be ideal,

$$J_i = \frac{P_g}{\sqrt{2\pi m k_B T_0}} ,$$

where P_g is the equilibrium pressure in the gas and m the mass of the He atom, while detailed balance implies

$$J_o = \frac{P_f}{\sqrt{2\pi m k_B T_f}} ,$$

where $T_f(t)$ is the instantaneous temperature of the film, and $P_f(t)$ is the pressure of the vapor that would be in equilibrium with the film at temperature T_f and coverage $n(t)$. When heat is injected into the film at a rate dU/dt, and it is assumed that this film remains in quasiequilibrium, conservation of energy requires that

$$\frac{dU}{dt} = C_N \frac{dT_f}{dt} + (\mu_f + T_f \bar{S}_f)\frac{dn}{dt} + \sigma(Q_o - Q_i) . \tag{3}$$

Here, the first term on the right-hand side, with C_N the heat capacity at constant coverage, accounts for the heat needed to raise the film's temperature; the second term, with $\hat{S}_f$ the partial molar entropy of the film, is the latent heat carried away by desorption, while Q_o and Q_i represent the outgoing and incoming fluxes of kinetic energy, assumed to be given by

$$Q_o = 2k_B T_f J_o$$

and

$$Q_i = 2k_B T_0 J_i .$$

From the point of view presented here, Eqs. (2) and (3) govern the time evolution of the film's coverage and temperature. To complete the equations and evaluate the coefficients, the film is assumed to have the properties of a thin slab of incompressible bulk liquid helium. This means that the adsorption isotherm is then given by the Frenkel-Halsey-Hill (FHH) equation

$$\mu_f(T,n) = \mu_l(T) + \Delta V_{\rm ext}(n) , \tag{4}$$

where $\mu_l(T)$ is the chemical potential of bulk liquid helium in coexistence with its vapor at temperature T. The excess van der Waals potential of the substrate, $\Delta V_{\rm ext}$, is taken to be

$$\Delta V_{\rm ext} = -\gamma/\delta^3 , \tag{5}$$

with δ, the film thickness, related to n by the liquid den-

sity, ρ_l, and where γ is characteristic of the helium-substrate system. Since the gas is ideal, Eq. (4) may be reexpressed as

$$P_f(T,n)=P_l(T)e^{\Delta V_{\rm ext}/k_B T}\ , \tag{6}$$

which relates the vapor pressure of the film at finite coverage to the vapor pressure of bulk liquid helium at the same temperature.

In a pulsed desorption experiment, energy dissipated in an Ohmic heater escapes partially into the helium film via Kapitza boundary resistance, R_K, and partially into a phonon-transparent sapphire crystal via boundary resistance R_c. The part that escapes into the helium becomes dU/dt of Eq. (3). As an order of magnitude approximation, all parameters (R_K, C_N, etc.) are evaluated from bulk liquid properties, including most importantly the sticking coefficient, σ, which is taken to be constant and equal to 1.[22] The resulting equations are then linearized for small departures from equilibrium. Defining the reduced dynamical variables

$$\chi(t)=[\delta_f(t)-\delta_0]/\delta_0$$

and

$$\theta(t)=[T_f(t)-T_0]/T_0\ ,$$

where δ_0 and T_0 are the initial undisturbed values, then, for χ and $\theta \ll 1$, Eqs. (2) and (3) reduce to

$$j=a\frac{d\theta}{dt}-b\frac{d\chi}{dt}+c\theta\ , \tag{7}$$

$$\frac{d\chi}{dt}=f\chi+g\theta\ . \tag{8}$$

These are coupled linear differential equations with constant coefficients (a,b,c,f,g,j) to be evaluated from existing data, and the energy deposited in the metallic heater, as discussed in Ref. 10.

In analyzing the behavior of Eqs. (7) and (8), it turns out that the most important experimental parameter is P_g, the preexisting gas pressure. For one thing, P_g governs the rate of exchange of both mass and energy between film and vapor. For another, it can vary over many orders of magnitude, while all other quantities affecting the coefficients vary relatively slowly. In practice, the experimental range of P_g was 10^{-3}–10^{-9} Torr.

Under these actual experimental conditions, the solutions of Eqs. (7) and (8) yield a particularly simple picture of desorption. It was found that the film temperature jumps rapidly to its steady-state value, essentially equal to T_s, while desorption proceeds much more slowly, with a time constant τ given approximately by

$$\tau=\frac{6\times10^{-12}}{T_0^{2.5}}e^{-\mu_0/k_B T_0}\ \text{sec}\ . \tag{9}$$

By contrast, the experiments of Sinvani *et al.*[7] could be parametrized by

$$\tau\approx10^{-9}e^{-2\mu_0/3k_B T_s}\ \text{sec}\ , \tag{10}$$

with the data taken in the limit $T_s \gg T_0$ (i.e., $\theta \gg 1$). Nevertheless, in spite of differences between these formulas, if the experimental result was extrapolated to the limit $T_s=T_0$, reasonably good numerical agreement between these time constants was found. Of course, this crude agreement could be considered no more than suggestive inasmuch as Eq. (9) states the dependence of the time constant on *initial* temperature for a film negligibly perturbed from equilibrium, whereas Eq. (10) describes the result for a variety of *final* film temperatures, all arrived at from the same equilibrium starting point. In other words, the predictions of the linearized theory and the parametrization of the data refer to explicitly different sets of experimental boundary conditions.

To make a more realistic appraisal, either the full, nonlinear equations would have to be solved in detail, or the experiments would have to be pushed to very small values of θ and the dependence of τ on initial temperature studied. There were, however, serious obstacles to each of these procedures.

In principle, the nonlinear equations could be integrated numerically (and this had been done in a few special cases), but there was good reason to doubt whether the results could be meaningfully compared to the experiments. First, considerable evidence accumulated that under the extreme conditions of the experiments, collisions between desorbing atoms affected the results in ways that rendered the interpretation of the existing data problematic and which, naturally, the model could not account for. Second, the basic assumption of the model, that the film evolves through a sequence of states of internal equilibrium, might not be entirely justified when the substrate temperature was forced to jump by as much as 10 K in a few nanoseconds. On the other hand, pushing the experiments into the near-linear regime, $\theta \ll 1$, did not appear to be feasible. Very few atoms would be desorbed in such an experiment, and the experimental signal is proportional to the net rate of desorption.

In the present work we have adopted a combined strategy of improving both theory and experiment. The experiments have been performed at small but nonnegligible θ, obviating the objections above, but still requiring solutions to the nonlinear equations. We have also worked out techniques for finding dependable approximate solutions to the nonlinear equations. As we shall see in the following sections, this combination not only permits a realistic comparison of theory and experiment, it also affords considerable insight into the behavior of both of them.

III. THE NONLINEAR THEORY

In this section we discuss how Eqs. (2) and (3) may be analyzed without being limited to small departures from equilibrium. That analysis is greatly facilitated by the fact that, when the preexisting gas pressure is sufficiently low, rapid heating of the substrate causes the temperature of the film to jump quickly to its final temperature, leaving desorption to take place isothermally and much more slowly. That behavior, which was previously ob-

served for small departures from equilibrium, turns out also to occur for larger ones. The physical reason is that, according to detailed balance, when the gas pressure is low, so is the rate of desorption, leaving no mechanism for the film to get rid of the energy flowing into it from the substrate. It therefore warms until it reaches nearly the temperature of the substrate, at which point the net energy flow slows down to the rate that desorption can manage to carry away.

That observation suggests a procedure for simplifying the equations. Rather than examine the case of small θ and χ, we look at the limit of small P_g for arbitrary θ and χ. Technically, the analysis requires the use of singular perturbation theory, as discussed in detail in Ref. 23, but the results are particularly simple. If the substrate is not heated too violently, the film temperature jumps to its final value T_s, equal to the substrate temperature, in a time so short that the film thickness can be taken to be undisturbed, and this result is insensitive to the precise values chosen for C_N and R_K. Desorption then proceeds isothermally, according to the equation

$$-\frac{dn(t)}{dt}=\frac{P_f(T_s,n)}{\sqrt{2\pi m k_B T_s}}-\frac{P_f(T_0,n_0)}{\sqrt{2\pi m k_B T_0}}\ , \tag{11}$$

which arises from Eq. (2) with $\sigma=1$.

Approximating $P_f(T,n)$ by means of the FHH equation of state, as given in Eqs. (5) and (6), Eq. (11) becomes a highly nonlinear differential equation for $n(t)$ that cannot be integrated analytically. However, numerical solutions, compared to numerical integrations of the full, coupled differential equations for $n(t)$ and $T_f(t)$, give excellent agreement for P_g as high as 10^{-3} Torr, i.e., over the entire experimental range of P_g. A typical example of the results is shown in Fig. 1, where numerical integrations of the full and approximate equations are compared for $P_g=10^{-5}$ Torr, $T_0=3.5$ K, and $\delta_0=0.8$ layers. In either scheme nearly all of the temperature change occurs in less than 100 nsec, while desorption evolves over some microseconds.

Additional insight can be gained by considering equations of state other than the FHH isotherm. If $P_f(T,n)$ were a linear function of n, Eq. (11) would have a simple exponential time dependence with a single time constant even for large disturbances from equilibrium. For example, if the adsorbate were a submonolayer classical ideal gas bound with energy ε_0 to a smooth substrate, the equation of state would be

$$P_f(T,n)=\left[\frac{n}{\beta\Lambda}\right]e^{-\beta\varepsilon_0}\ , \tag{12}$$

where $\beta=(k_B T)^{-1}$ and $\Lambda=h/(2\pi m k_B T)^{1/2}$. Then Eq. (11) is of the form

$$-\frac{dn}{dt}=k_d n-c\ ,$$

where k_d is the desorption rate constant, and c is a constant term representing readsorption. The solution is

$$n(t)-n_0=(n_{ss}-n_0)(1-e^{-k_d t})\ ,$$

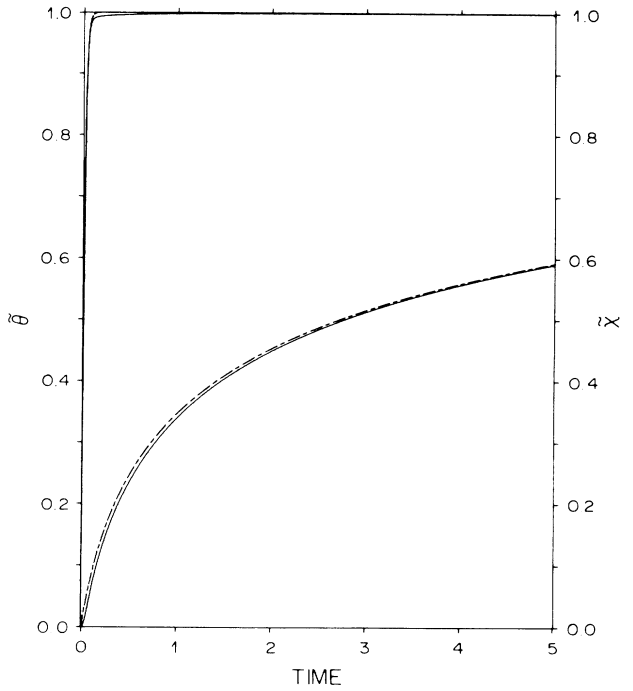

FIG. 1. Comparison of exact (solid lines) and approximate (dashed lines) solutions to the bulk-continuum model for $T_0=3.5$ K, $P_g=10^{-5}$ Torr, and $\delta_0=0.8$ layers, when $T_s=5.25$ K. The dynamical variables are scaled to their steady-state values so that $\tilde{\theta}=\theta(t)/\theta_{ss}$ for the upper pair of curves, and $\tilde{\chi}=\chi(t)/\chi_{ss}$ for the lower pair. Time is in units of μsec.

where n_{ss} is the steady-state value, $n(\infty)$. The desorption time constant, $\tau=k_d^{-1}$, is

$$\tau=h\beta_s e^{\beta_s\varepsilon_0}\ ,$$

which has the activated form of Eq. (1).

The behavior of a film with a linear equation of state is sketched in Fig. 2. Starting at (n_0,T_0) the system jumps essentially instantaneously to (n_0,T_s), then follows the T_s isotherm to (n_{ss},T_s). For such a system, experiments involving large changes in n and T would still measure the mean dwell time (at T_s) typically calculated from microscopic theory [see Eq. (13) below]. This behavior would occur not only for the particular model represented by Eq. (12), but for any instance in which the adsorption energy is constant, and the adsorbed atoms or molecules do not interact with each other (this is known as Henry's law).

Unfortunately, Henry's law does not obtain in physisorption on real surfaces. Even on the most homogeneous surfaces, high-binding-energy sites dominate adsorption precisely in the limit of low coverage where Henry's law might be expected to apply. At higher coverage, interactions between adsorbate particles can cause various phase transitions and layer formation, leading to complicated behavior in the dependence of $P_f(T,n)$ on n. On less homogeneous surfaces, variation of the binding energy over the surface may smear out much of this structure, and $P_f(T,n)$ typically has a sigmoid shape,

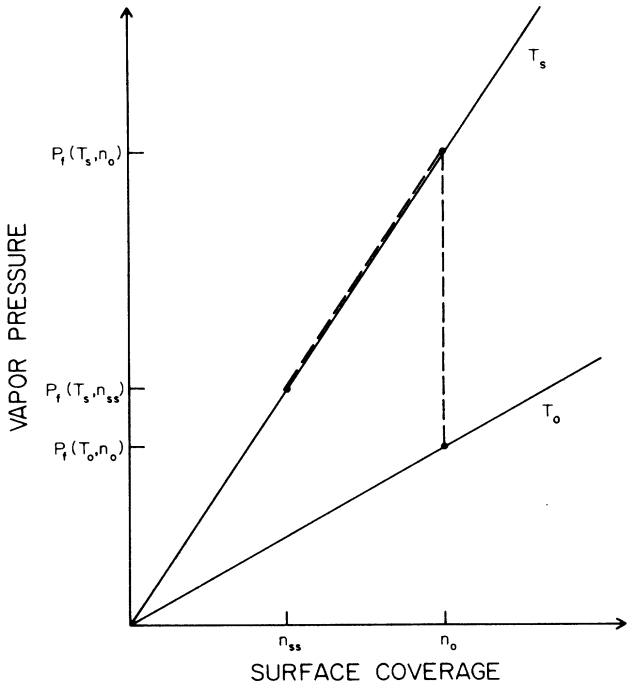

FIG. 2. Isothermal desorption of a two-dimensional classical ideal gas.

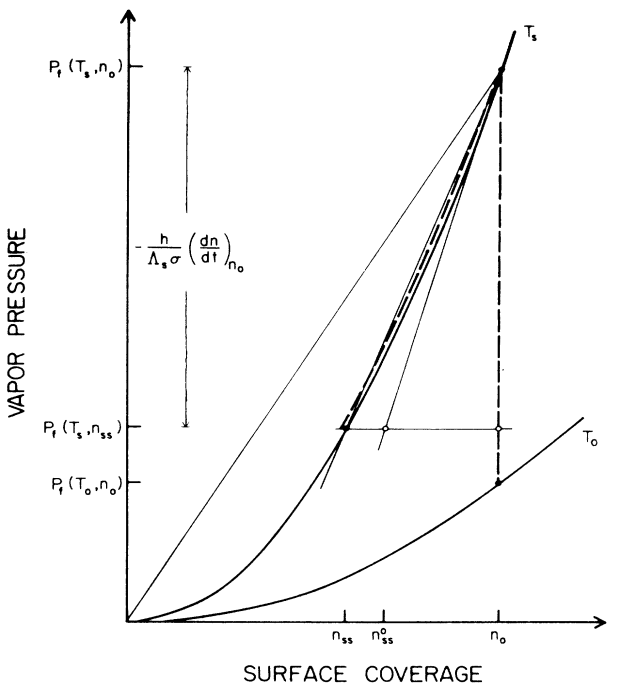

FIG. 3. Isothermal desorption for a system with positive curvature as defined in the text.

qualitatively similar to the Brunauer-Emmett-Teller (BET) formula. For either homogeneous or inhomogeneous substrates, the FHH equation, Eqs. (5) and (6), is expected to become valid for films of more than a few layers, provided the adsorbate wets the substrate, but it shares the same qualitative shape as the BET isotherm over the entire range of n.

Figure 3 indicates the situation when $P_f(T,n)$ is not linear. We have chosen to illustrate the case $\partial^2 P_f/\partial n^2 > 0$, which we shall refer to as having positive curvature. This is how both FHH and BET look in the low-coverage region. The dashed curve indicates the behavior of the system as it jumps from (n_0,T_0) to (n_0,T_s), and then follows the T_s isotherm down to (n_{ss},T_s). Depending on how this behavior is analyzed, one can identify four different kinds of time constants:

(1) The mean dwell time on a homogeneous surface is obtained by equating adsorption to desorption, as one would in equilibrium, and writing

$$\frac{n}{\tau(n)} = \frac{P_f(T_s,n)}{\sqrt{2\pi m k_B T_s}} \ . \tag{13}$$

This time is proportional to n/P_f, the inverse slope of the line drawn from $P_f(T_s,n)$ to the origin, and depends on the instantaneous coverage. For an inhomogeneous surface with a nonuniform distribution of binding sites,

$$\frac{n}{\tau(n)} = \sum_i \frac{n_i}{\tau_i(n_i)} \ ,$$

where n_i refers to the number in each type of site ($\sum_i n_i = n$) and τ_i is derived from the partial pressure $P_{fi}(T,n_i)$.

(2) If Eq. (11) is linearized for small $n - n_0$, but finite $T_s - T_0$, we obtain

$$-\frac{dn}{dt} = \text{const} + \frac{\partial P_f/\partial n}{\sqrt{2\pi m k_B T_s}}(n - n_0) \ . \tag{14}$$

This procedure yields an instantaneous, or local, linearized time constant, $\tau_{\rm lcl}(n_0)$, in the neighborhood of n_0 at temperature T_s. This time scale is proportional to the inverse slope of the tangent to the T_s isotherm at n_0, $(\partial n/\partial P_f)_{T_s,n_0}$, shown in the figure. One could visualize repeating this procedure at any point in the trajectory along the T_s isotherm leading to a succession of instantaneous time scales, $\tau_{\rm lcl}(n)$, and a continuous renormalization of the constant appearing in Eq. (14). Expressed in terms of the instantaneous chemical potential of the film, a general formula for this time scale, suggestive of Arrhenius-like behavior, is

$$\tau_{\rm lcl}(n) = \frac{h\Lambda_s^2}{\sigma}\left[\frac{\partial \mu_f}{\partial n}\right]_{T_s}^{-1} e^{-\mu_f(T_s,n)/k_B T_s} \ . \tag{15}$$

(3) The time constant in Eq. (9) arising out of the solution of the linearized (infinitesimal $T_s - T_0$) equations, Eqs. (7) and (8), is similarly governed by the inverse slope of the T_0 isotherm evaluated at n_0, $(\partial n/\partial P_f)_{T_0,n_0}$. This may also be written in a more general activated form by substituting T_0 for T_s and using the *equilibrium* value of the chemical potential in Eq. (15),

$$\tau=\frac{h\Lambda_0^2}{\sigma}\left[\frac{\partial\mu_f}{\partial n_0}\right]_{T_0}^{-1} e^{-\mu_f(T_0,n_0)/k_BT_0} . \quad (16)$$

(4) A fourth scale usefully characterizes the global time evolution of the film as it progresses down the T_s isotherm from n_0 to n_{ss}. Since the system is not exponential in time there is no single time constant, as we have seen above. Nevertheless, $n(t)$ behaves as shown in Fig. 4, rising at first and then bending over to an asymptote at n_{ss}. An experimentalist, obtaining data of this form, would be inclined (as Sinvani *et al.* were) to treat it as if it were a simple exponential, which it resembles qualitatively if there is not too much curvature on a logarithmic plot, and extract a single time constant. This is most conveniently done by extrapolating the initial slope the steady-state coverage n_{ss}, as shown in the figure. Accordingly, we define a global time constant, τ_{exp}, as

$$\tau_{exp}=\frac{n_0-n_{ss}}{-(dn/dt)_0} , \quad (17)$$

where n_{ss} is the solution of

$$T_s^{-1/2}P_f(T_s,n_{ss})=T_0^{-1/2}P_f(T_0,n_0) ,$$

and $(dn/dt)_0$ is the initial rate of desorption, given by

$$-\left[\frac{dn}{dt}\right]_0=\frac{P_f(T_s,n_0)}{\sqrt{2\pi mk_BT_s}}-\frac{P_f(T_0,n_0)}{\sqrt{2\pi mk_BT_0}} .$$

In terms of the figure, τ_{exp} is proportional to the inverse slope of the chord connecting the point (n_0,T_s) to (n_{ss},T_s). It depends on the total amount desorbed.

Thus, given a model (or experimental data) for the equation of state of the film, $P_f(T,n)$, the predicted values of τ_{exp} are easily found without solving the nonlinear differential equation, Eq. (11). Our discussion of the dynamics in terms of strictly geometrical properties of the equilibrium adsorption isotherm rests, however, on the assumption of a coverage-independent sticking coefficient. Should σ depend on n in an important way, then the connection with the equation of state becomes less direct as additional terms enter the definitions of τ_{lcl} and τ_{exp}.

In Fig. 5 we plot the calculated values of τ_{exp}, using the FHH equation of state, for a variety of initial conditions (see Table I for the relevant parameters.) Since the ordinate is logarithmic and is plotted versus T_0/T_s, this figure is comparable to the Arrhenius plots ($\log_{10}\tau$ versus $1/T_s$) that Sinvani *et al.* used to analyze their data. The result is an excellent straight line over decades of τ_{exp}, just as observed in these experiments. The intercepts of these curves give $\tau_0\approx10^{-11}$ sec, and the slopes give a characteristic energy somewhere in the region between $|\mu_0|$ and $0.5|\mu_0|$, where μ_0 is the *equilibrium* chemical potential. The intercept of each curve with the axis $T_0/T_s=1$ is the solution for that set of initial conditions of the linearized equations, Eqs. (7) and (8).

In Fig. 6 we compare the predictions of the model with data from Sinvani *et al.* (open squares) and from our own experiments, described in the next section (solid squares). The agreement is quite good, especially for the more recent experiments, where T_0/T_s is closer to 1. Since the experimental films are less than about two lay-

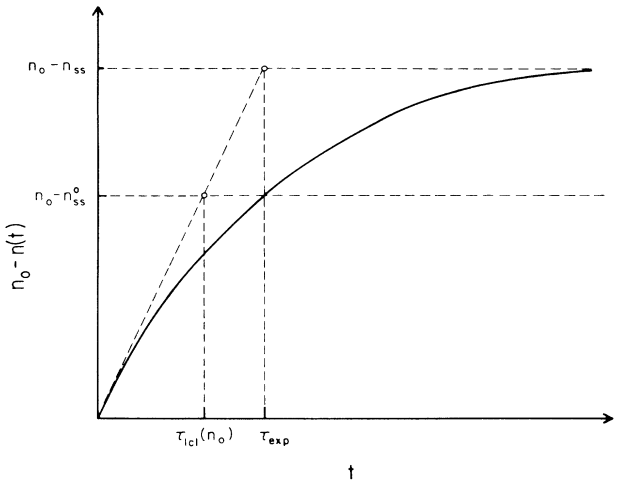

FIG. 4. Number desorbed per unit area vs time for isotherms with positive curvature.

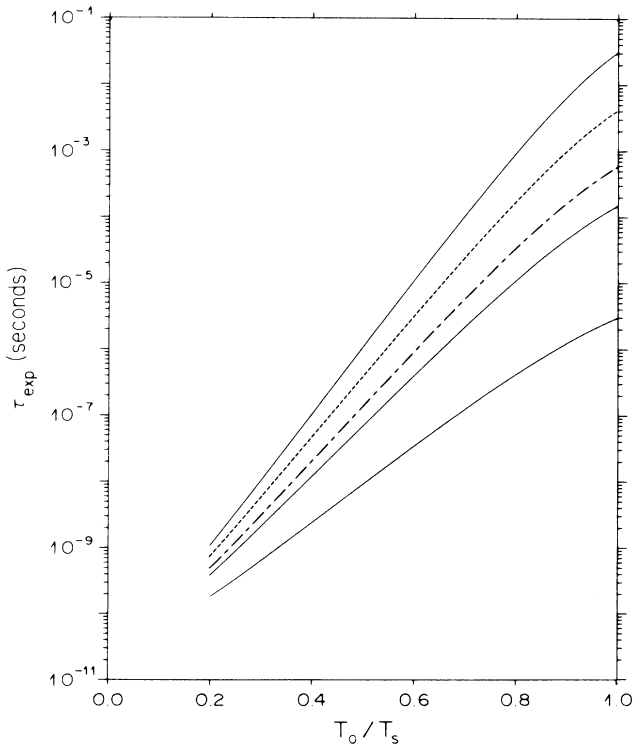

FIG. 5. Global time constant as a function of inverse substrate temperature for a variety of initial conditions. Bottom, middle, and top solid curves correspond to the first three rows of Table I, respectively. Broken and dashed curves represent rows 4 and 5.

TABLE I. Relevant parameters for the sequence of examples plotted in Fig. 5.

T_0 (K)	$-\mu_0$ (K)	P_g (Torr)	$-\mu_0/T_0$ (dimensionless)	n_0 (layers)
3.5	55	5.3×10^{-4}	15.7	0.87
3.5	70	7.3×10^{-6}	20.0	0.79
3.5	90	2.4×10^{-8}	25.7	0.72
2.0	40	1.8×10^{-6}	20.0	0.97
1.0	20	3.1×10^{-7}	20.0	1.33

ers thick though, the FHH equation of state cannot be very accurate, and the agreement appears to be fortuitous. Nevertheless, the qualitative fact that FHH has positive curvature in this low-coverage regime seems to be more important in accounting for the data than its quantitative accuracy.

Note that the two sets of initial conditions (n_0 and T_0) shown in Fig. 6 are apparently quite different, yet both sets of experiments and theoretical predictions fall on nearly the same curves. That is because these initial conditions do have, very nearly, the same ratio of μ_0 to T_0, which means, in effect, (almost) the same P_g, and this scaling is generally found to hold when the resulting $\tau_{\rm exp}$ are plotted against the dimensionless ratio, T_0/T_s.[23]

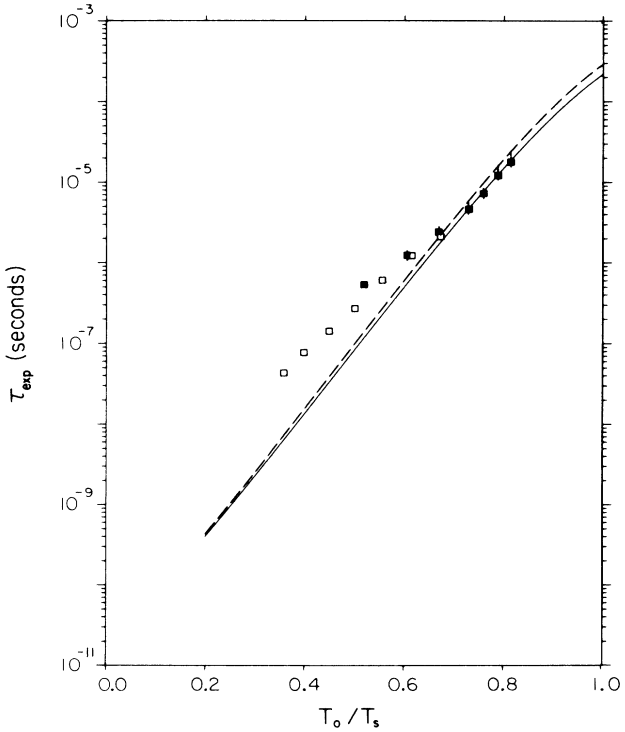

FIG. 6. Comparison of the global time-constant data and continuum-model predictions from this work for $T_0=2.10$ K, $-\mu_0=40$ K (solid squares and solid line, respectively) with the data of Sinvani *et al.* for $T_0=3.48$ K, $-\mu_0=72$ K, and our corresponding model predictions (open squares and dashed line).

IV. EXPERIMENT

As mentioned above, the experiments were essentially similar to others previously reported by our laboratory, except that they were designed to use much smaller disturbances from equilibrium. The desorption substrate was an evaporated Ohmic heater on the surface of a phonon-transparent sapphire crystal, and the detector was a superconducting transition edge tin bolometer, on a separate sapphire wafer, 1.25 mm above the heater. The experiment consists of pulsing the heater periodically and observing the resulting signal carried to the bolometer by desorbed helium atoms. A new cryostat was constructed, carefully designed for low heat leak and long liquid-helium–bath life, in order to facilitate systematic data collection. In addition, two important changes from previous practice were the use of a relatively large area heater to enhance the signal due to small heater pulses, and a new, more efficient, system for data retrieval, storage and analysis.

The heater was a 500-Å-thick nichrome film evaporated directly onto the optically polished surface of a sapphire single crystal. Scanning electron micrographs indicate the surface roughness of the sapphire to be less than 250 Å. The bottom of the crystal is immersed in the helium bath, and the top, on which the heater is evaporated, forms the floor of an oxygen-free high-conductivity (OFHC) copper adsorption cell, to which the crystal is sealed by means of an indium gasket. The bolometer wafer is secured in place by sapphire spacers attached by means of Apiezon vacuum grease, and the cell also contains 0.175 g of Grafoil (surface area $\sim4\times10^3$ cm^2) so that an adsorbed monolayer on all surfaces in the cell corresponds to a conveniently measurable quantity of gas. The surface area of the heater was 1.10 mm^2 (about 10 times larger than those previously used in our laboratory) and its resistance (47.5 Ω) was well matched to the 50-Ω impedance of our transmission lines.

The bolometer was a 2000-Å Sn evaporated film, photolithographically fashioned into a serpentine ~0.3 mm on a side (total area ~0.1 mm^2). It could be operated at any temperature below the superconducting critical temperature of tin, $T_c\approx3.7$ K, with the aid of a magnetic field perpendicular to the plane of the bolometer. In a separate series of experiments, it has been found that this type of bolometer has a peak sensitivity of ~200 V/W at a typical bias current of ~1 mA, surprisingly independent of operating temperature once optimal biasing conditions (magnetic field and current) are determined.[24]

When the heater, initially at temperature T_0, is suddenly pulsed with electrical power W, it is assumed to come to a temperature T_h given by

$$W=C_h\frac{dT_h}{dt}+\sigma_c(T_h^4-T_0^4)\ .$$

C_h is the heat capacity of the nichrome film[25] and σ_c is the analog of the Stephan-Boltzmann constant for radiating phonons into the sapphire substrate, calculated from the elastic constants of both heater and substrate

assuming perfect interface bonding between them.[26,27] The coefficient σ_c is related to R_c, the Kapitza thermal boundary resistance of the heater/sapphire interface, by $\sigma_c^{-1}=4T_0^3R_c$. With this assumption, the heater reaches a steady-state temperature

$$T_s=(W/\sigma_c+T_0^4)^{1/4} \tag{18}$$

in a maximum time given roughly by

$$\tau_h \sim \frac{7\times10^{-8}}{T_0^2} \text{ sec} .$$

In estimating this time, we have ignored heat lost into the helium film. As we saw in the preceding section, that heat causes the helium film to rise to essentially the same temperature, T_s, in a comparably short time after which little further heat exits by that route. The net result is that heater and helium film may both be thought of as jumping to temperature T_s in a time negligibly short compared to desorption times, and that Eq. (18) should be reliable for calculating T_s within the scope of the acoustic-mismatch model.

A block diagram of the instrumentation is shown in Fig. 7. Desorption is caused by heater pulses of 10 V amplitude, 5 nsec risetime, and width $t_p \geq 30$ nsec, attenuated as necessary in 1-dB steps. A synchronous reference signal activates the data-acquisition electronics. The bolometer output is coupled to a room-temperature wide-band (dc–70 MHz) preamplifier via a 100-μF tantalum capacitor which, in combination with the 50-Ω input impedance of the preamplifier, creates a high-pass filter eliminating the dc offset of the bolometer biasing circuit while allowing signals up to several hundred μsec duration to be recovered with minimum distortion.

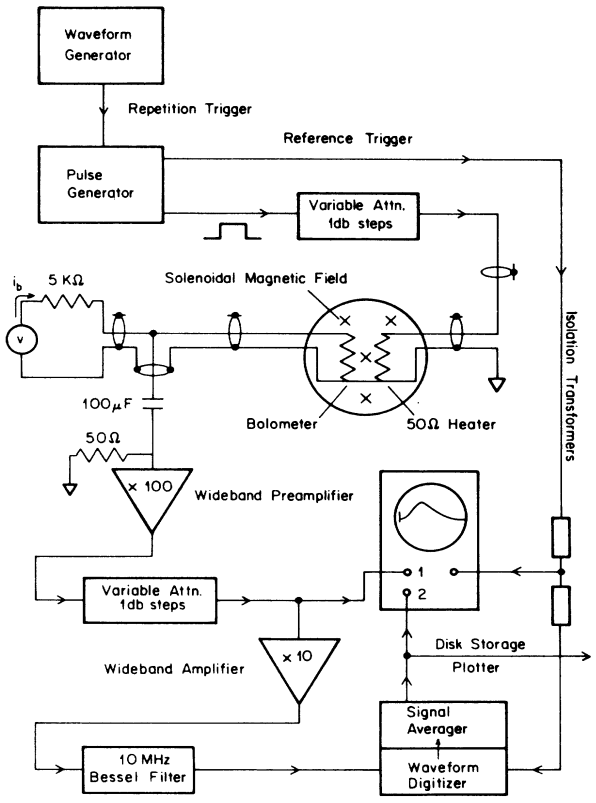

FIG. 7. Electronics for the desorption time-constant measurements.

The observed broadband noise of the system, dominated by the amplifier electronics, is ~ 15 μV rms referred to the preamplifier input (equivalent to $\sim 7\times10^{-8}$ W heat input to the bolometer signal before signal averaging). To limit this noise by reducing unnecessary bandwidth, a low-pass filter, carefully chosen to preserve both the amplitude and phase of all important Fourier components of the signal, is needed. A convenient choice proved to be a two-pole, 10-MHz Bessel filter synthesized from a single capacitor and inductor.[28]

Signal recovery and signal-to-noise enhancement were accomplished by means of a LeCroy 3500 system serving as a waveform digitizer and signal averager. On each trigger, the entire bolometer signal, as a function of time after the pulse, is digitized as typically 1024 or 2048 points at 40-nsec intervals with eight-bit nominal resolution (as much as ten-bit effective resolution was possible after signal averaging). The signal-averager throughput (700×1 kbyte samples per second) is fast enough so that it is almost never the factor limiting pulse repetition rates. This represents an enormous gain in signal-averaging efficiency over the previous method, a boxcar integrator, which effectively measures only a small gated portion of the signal from each pulse. The digitized and averaged signal may be stored on floppy disk and recalled for later viewing and manipulation.

In essence, the experiments probe the kinetics of both desorption and adsorption by observing the signal as a function of the pulse duration, t_p, and the pulse repetition time t_r. Varying t_r (or equivalently, $\nu_r=1/t_r$) probes readsorption or recovery of the film. In particular, when t_r is sufficiently long, $t_r > t_{rc}$, the film generally regains thermodynamic equilibrium between pulses (unless it is on a flat portion of the isotherm where $dP_f/dn=0$), as shown by the fact that the signal becomes independent of t_r. Since t_{rc} depends on the preexisting gas pressure P_g, it can be used to measure that important parameter (with an uncertainty of $\sim 30\%$) and hence also the equilibrium chemical potential, μ_0 (since μ_0 depends logarithmically on P_g, its uncertainty is much smaller, of order a few percent).[29] The parameter t_{rc} also serves to limit the maximum repetition rate of the experiment for signal-averaging purposes. For thin films and/or low temperatures, t_{rc} may be as large as 10 sec in some cases, so that the efficient digital signal averaging described above is particularly important.

All experiments are performed at sufficiently low P_g to ensure that the mean free path in the preexisting gas is long compared to the distance between heater and bolometer. A more difficult problem concerns collisions between desorbing atoms. Unless the mean number of collisions per atom can be kept small compared to 1, backscattering of desorbed atoms into the film and collision-induced forward focusing of desorbed atoms

into the fixed solid angle subtended by the detector[30] may well affect the time evolution we are trying to measure. This clearly appears to have been the case in previous measurements.[7] The mean number of collisions per atom for a typical run has now been estimated to have been about 5.[31] For the small departures from equilibrium used in the present experiments, the times characterizing desorption can be longer than the mean transit time of atoms between the heater and bolometer, t. In this case, a rough estimate of the number of collisions expected per atom, ν, is given by

$$\nu \approx \Delta \frac{t}{\tau} , \tag{19}$$

where τ is a time characterizing the desorption, and Δ is the number of monolayers in the film.[32] Typical values for our films are $\Delta \sim 1$ ML (monolayer), $t \sim 10$ μsec, and $\tau \geq 5$ μsec.

To summarize the experimental situation, the work reported here improves over previous observations mainly by allowing analysis of signals due to smaller disturbances from equilibrium. This permits a more direct comparison to theory principally because collision effects are considerably reduced.

As mentioned above, the purpose of the new data gathered for this study was to probe the kinetics of desorption and adsorption by varying the pulse width, t_p, the repetition rate, t_r, and the heater power (and hence T_s), all at lower heater power than had been used before. To keep this survey manageable, all the data had the same initial conditions, $T_0 = 2.09$ K and $P_g = 5.8 \times 10^{-6}$ Torr corresponding to $\mu_0 = -40$ K and a mean free path in the undisturbed gas of 94 mm (about 80 times the source-detector separation.) The pressure P_g was deduced from the critical repetition rate at maximum power ($t_{rc} = 14$ msec), as discussed above, and checked periodically throughout the experiment. The cell was filled with 1.69 STPcc of helium gas, one-third admitted at 77 K and the rest bled in at 4.2 K. The cell was then slowly cooled to T_0, and maintained there for a full week before any data were taken. The data comprised nearly 1000 waveforms, each signal averaged over 1000 or more triggers. The values of T_s that were used, and the parameters used in calculating them, are summarized in Table II.

We do not know the mean equilibrium helium film thickness on the nichrome heater in these experiments, but we can assign an upper limit of 1.2 ML which is the helium film thickness on the more strongly absorbing Grafoil substrate at our equilibrium values of T and μ.

Some examples of typical bolometer signals at low heater power are shown in Fig. 8. The signal is believed to be given by $A_d K S(t)$, where A_d is the detector area, K the sensitivity in volts per watt, and $S(t)$ the rate at which energy is deposited per unit area at the bolometer. This can be put in the form

$$S(t) = \int_0^t dt' \, \dot{n}(t') \int_{A_s} d^2 r' \, S_0(\mathbf{r} - \mathbf{r}', t - t'; \beta_s) , \tag{20}$$

when the desorption is isothermal and the sticking probability independent of coverage. Here, $\dot{n}$ is the instantaneous *excess* rate of desorption, at time t' from point $\mathbf{r}'$, above the equilibrium value that would otherwise have originated from the heater surface. The second integral spans the area of the heater, whereas the bolometer is considered to be a point detector situated at $(x,y,z) = (\mathbf{r},z)$. Assuming no collisions, and constant sticking coefficient σ_d at the bolometer,

TABLE II. Heater temperature T_s calculated as a function of pulse power W, from Eq. (18). $W_{max} = 2$ W/1.10 mm^2, $1/\sigma_c = 6800$ K^4 mm^2/W, and $T_0 = 2.095$K.

W/W_{max} (dB)	T_s (K)	T_0/T_s	Uncertainty due to a 10% imprecision in W/σ_c
0	10.549	0.199	±0.005
−17	4.038	0.519	±0.012
−20	3.457	0.606	±0.013
−22	3.140	0.667	±0.013
−24	2.877	0.728	±0.013
−25	2.764	0.759	±0.013
−26	2.663	0.787	±0.012
−27	2.575	0.814	±0.011

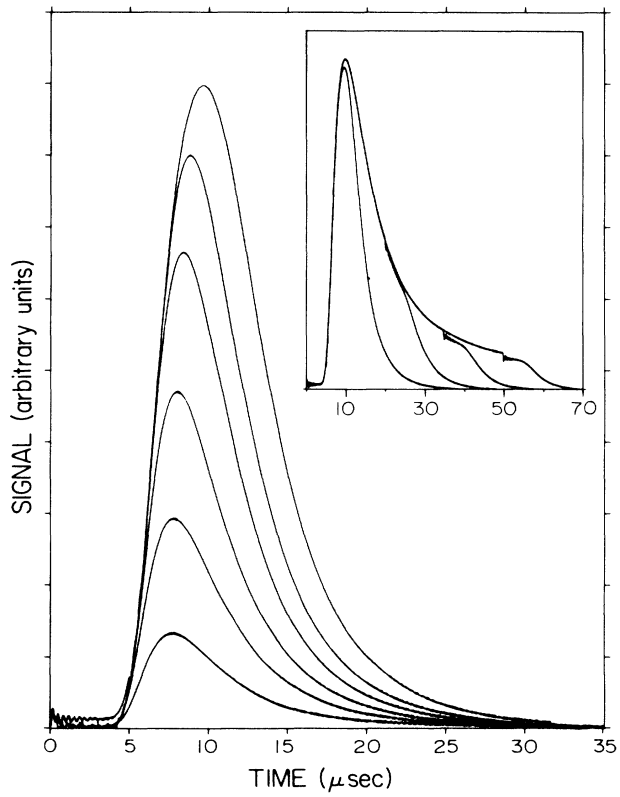

FIG. 8. $S(t)$ vs t, as a function of t_p, for $T_s = 2.88$ K and $\nu_r = 70$ Hz. Main figure: $t_p = 0.35$, 0.70, 1.2, 2.0, 3.0, and 5.0 μsec. Inset: $t_p = 5.0$, 20, 35, and 50 μsec.

$$S_0(\mathbf{r}-\mathbf{r}', t-t'; \beta_s) = \sigma_d \left[\tfrac{1}{2} m \frac{|\mathbf{r}-\mathbf{r}'|^2}{(t-t')^2} + E_b \right] \times N_0(\mathbf{r}-\mathbf{r}', t-t'; \beta_s) , \quad (21)$$

where the term in large parentheses on the right-hand side is the kinetic plus binding energy deposited by an incident atom. The signal is presumed weak enough for the coverage on the bolometer to be essentially undisturbed, so that E_b remains constant. N_0 is a propagator from heater to bolometer given by

$$N_0(\mathbf{r}-\mathbf{r}', t-t'; \beta_s) = \frac{z^2}{(t-t')^5} \frac{(\beta_s m)^2}{2\pi} \times e^{-\beta_s m |\mathbf{r}-\mathbf{r}'|^2/2(t-t')^2} \Theta(t-t') , \quad (22)$$

where $\beta_s = (k_B T_s)^{-1}$, T_s is the temperature of the desorbing atoms, and $\Theta(t-t')$ is a unit step function ensuring that causality is obeyed, permitting the integration over t' in Eq. (20) to be extended to infinity. Expressed in words, $S(t)$ is a consequence of the instantaneous desorption rate, $\dot{n}(t')$, coupled with the dynamical fact that higher-energy atoms arrive sooner and deposit more energy, and the geometric fact that the path length depends on where on the heater the atom originated from. To write $S_0(t)$ in the form of Eq. (21), we have assumed that the desorption is isotropic. A more detailed formalism would take into account that both desorption and adsorption are governed (through detailed balance) by sticking coefficients that may be velocity dependent and hence not isotropic.

There are a few experimental strategies available to help simplify the analysis of how these data depend on the pulse width, t_p. One, introduced by Sinvani *et al.*, is to notice that in curves like those of Fig. 9, taken at relatively high heater power, the maximum signal height appears to saturate as a function of the pulse width, t_p. This presumably means net desorption runs its course and ceases when the pulse has been on for a sufficiently long time. Assuming the peak height approaches saturation in a simple exponential manner as a function of t_p, these authors used this method to find the characteristic time for the desorption steady state to be reached. However, given the factors that may influence $S(t)$ that are especially evident at the lower powers in Fig. 8, a more dependable procedure for finding a time to compare to the predictions of the preceding section would require first isolating the total excess desorption in a pulse,

$$\Delta n(t_p) = \int_0^{t_p} \dot{n}(t')dt' . \quad (23)$$

This suggests that we analyze the area of the signal, $\int S(t)dt$, rather than $S(t)$ itself:

$$\int_0^\infty dt\, S(t) = \int_0^\infty dt'\, \dot{n}(t') \times \int_{A_s} d^2r' \int_0^\infty dt\, S_0(\mathbf{r}-\mathbf{r}', t-t'; \beta_s) .$$

But,

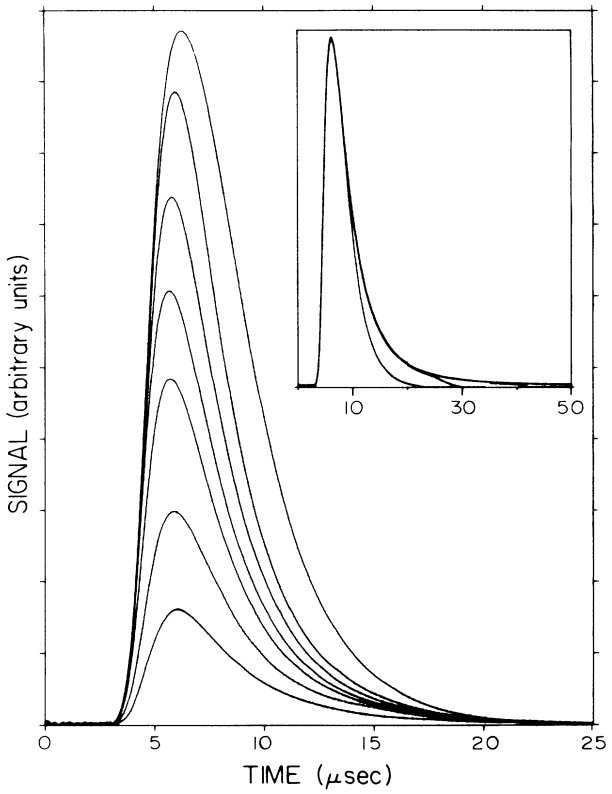

FIG. 9. $S(t)$ vs t, as a function of t_p, for $T_s = 4.04$ K and $\nu_r = 70$ Hz. Main figure: in ascending order, $t_p = 0.10$, 0.15, 0.25, 0.35, 0.50, 0.90, and 3.0 μsec. Inset: $t_p = 3.0$, 20, 35, and 50 μsec. For comparison, full scale is roughly 7 times that of Fig. 8.

$$\int_0^\infty dt\, S_0(\mathbf{r}-\mathbf{r}', t-t'; \beta_s) = \sigma_d (2k_B T_s + E_b) \int_0^\infty dt\, N_0(\mathbf{r}-\mathbf{r}', t-t'; \beta_s) \quad (24)$$

and

$$\int_0^\infty dt\, N_0(\mathbf{r}-\mathbf{r}', t-t'; \beta_s) = \frac{1}{\pi} \frac{z^2}{|\mathbf{r}-\mathbf{r}'|^4} . \quad (25)$$

These last two steps are possible because the various components of S_0 and N_0 depend only on the elapsed time, $t-t'$, not on absolute time t. In effect, Eq. (24) replaces an integral over kinetic energies with the mean kinetic energy of the desorbed atoms, $2k_B T_s$, and the right-hand side of Eq. (25) is just a geometric factor for all those emitted particles that will eventually strike the detector.

A problem remains, however, in that

$$\int_0^\infty \dot{n}(t')dt' = 0 .$$

This is true because after a desorption pulse is turned off, the film eventually returns to equilibrium. For a long time after the pulse, the heater desorbs fewer atoms than it would in equilibrium, the bolometer receives fewer than the rate that makes its equilibrium reading equal to zero, and the signal actually becomes negative.

In practice, this problem can usually be solved. In our experiments it is almost always possible to find an intermediate time, t_I, such that $t_I - t_p$ is large compared to the characteristic width of S_0, so that all particles desorbed in the pulse have plenty of time to reach the bolometer, but that is still very short compared to the time required for the film to return to equilibrium after the pulse. Then,

$$\int_0^{t_I} S(t)dt = \Delta n(t_p) \times \left[\sigma_d(2k_B T_s + E_b)\frac{1}{\pi}\int_{A_s} d^2r' \frac{z^2}{|\mathbf{r}-\mathbf{r}'|^4}\right]. \tag{26}$$

The choice of t_I is almost always obvious from the data themselves (e.g., 35–70 μsec in Fig. 8). It must be borne in mind, however, that there are conditions—such as desorption for nearly infinitesimal temperature variations, or for very short pulse widths—under which it may not be possible to separate cleanly the time scales corresponding to desorption, adsorption, and the width of the propagator, which is necessary for this to be a viable means of reconstructing $\Delta n(t_p)$.

One other point we have ignored in formulating Eq. (20) the way we did is the fact that atoms that would have desorbed from the heater during time t_p, if the heater had not been pulsed, would have had temperature T_0 rather than T_s. This introduces an error which is usually small, and the area under $S(t)$ is strictly proportional to $\Delta n(t_p)$ provided

$$\left[\frac{\dot{n}_{\rm eq} t_p}{\Delta n(t_p)}\right]\frac{2k_B(T_s - T_0)}{2k_B T_s + E_b} \ll 1 , \tag{27}$$

where $\dot{n}_{\rm eq}$ is the desorption rate in equilibrium. This condition is best satisfied for small disturbances (small $T_s - T_0$), thin films (large E_b), and if t_p is not too much longer than the time to reach the steady state.

As an example of this kind of analysis, we show in Fig. 10 plots of $\int_0^{t_I} S(t)dt$ versus t_p for calculated substrate temperatures $T_s = 3.46$ K (upper curve) and $T_s = 2.88$ K (lower curve). In both cases, Eq. (27) is well satisfied, so that the ratio of the points at any t_p should be equal to the ratio of the values of $\Delta n(t_p)$.

These data exhibit many of the features of the model discussed in the preceding section. For example, both curves extrapolate to zero signal at a finite $t_p \sim 50$–100 nsec. This is the expected time scale for both heater and helium film to reach their final temperature, and corresponds to the difference between the full numerical integration and the approximate model in Fig. 1. After this time the curves have a slope proportional to the rate of change of surface coverage $\dot{n}$, higher for the higher substrate temperature, and at long t_p the curves become largely independent of pulse width and saturate. In practice, there is some difficulty in finding the saturation value of $\int S\,dt$ for a moderate-strength bolometer signal near steady state, owing to the continuing arrival of hotter gas atoms than would arrive at equilibrium, and

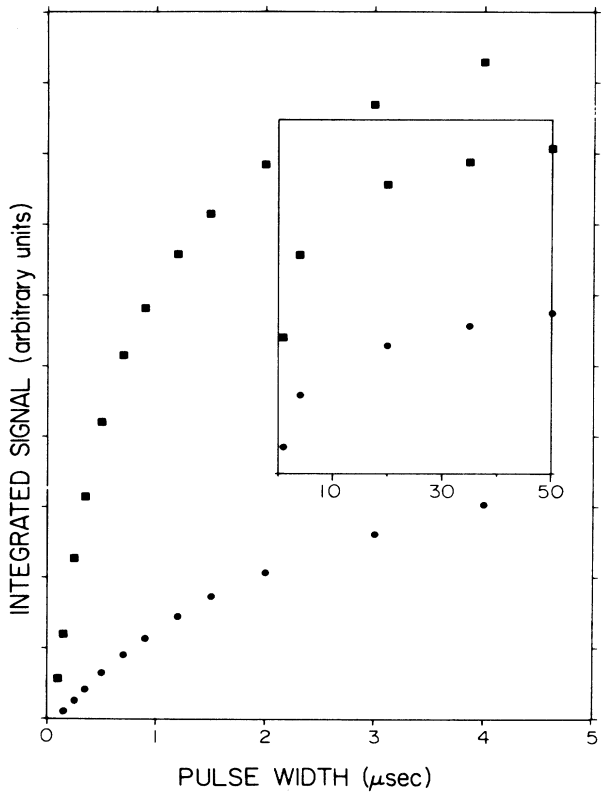

FIG. 10. $\int_0^{t_I} dt\, S(t)$ vs t_p for $T_s = 3.46$ K (squares) and $T_s = 2.88$ K (circles). Same pulse-width sequence applies in both cases, excepting the first point at $t_p = 0.10$ μsec, which is indicated only for the higher temperature. Full scale in the inset is 1.5 times that of the main figure.

to small heat leaks from heater to bolometer by paths other than desorption. Nevertheless, the qualitative similarity to Fig. 4 is clear, and quantitative analysis is not difficult.

To get a clearer picture of the quantitative behavior of the data, we plot $\log_{10}\dot{n}(t)$ versus t for the data at $T_s = 3.46$ K, in Fig. 11. The first five points fit a pure exponential for $n(t)$, with characteristic time $\tau = 0.51$ μsec, but subsequent points depart from that behavior. According to the arguments of Sec. III, $\tau = 0.51$ μsec characterizes the solution of Eq. (15) (it is the local time constant near equilibrium coverage), and the subsequent departure from exponential behavior in $n(t)$ is due to nonlinearity of the equation of state of the film. The inset of Fig. 11 shows

$$\tau_{\rm lcl}(n(t)) = -\frac{(dn/dt)}{(d^2n/dt^2)}$$

versus t, constructed from second differences of the data [the equivalence of this definition of $\tau_{\rm lcl}(t)$ to our previous one, in terms of the instantaneous slope of the adsorption isotherm, is demonstrated in Ref. 23]. In agreement with the main figure, $\tau_{\rm lcl}$ is constant at ~ 0.5 μsec for the first 1 μsec of desorption, but then increases as the film evolves. This increase is consistent with the qualitative curvature of the isotherm depicted in Fig. 3.

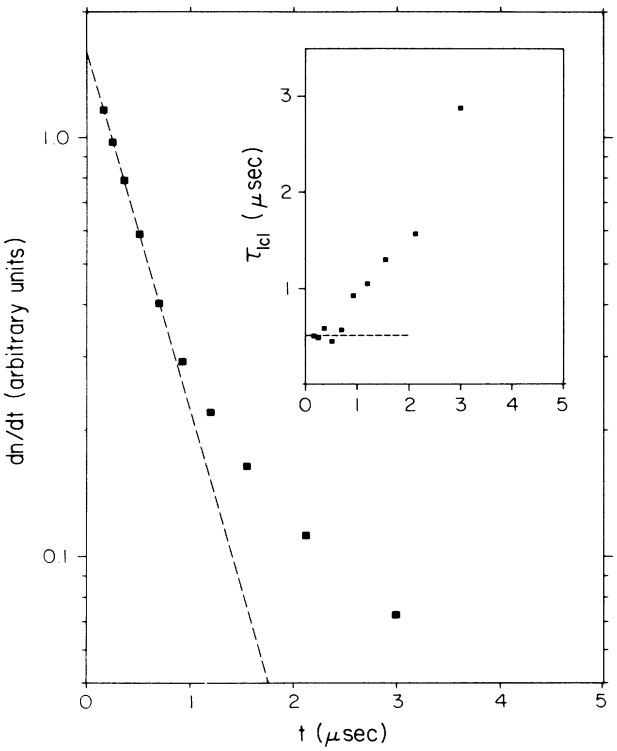

FIG. 11. Finite-difference approximation to the net rate of change of surface coverage with time plotted on a logarithmic scale for $T_s=3.46$ K. Straight line is an exponential fit with $\tau=0.51$ μsec. Inset shows a finite-difference approximation to the local time constant vs time on a linear scale.

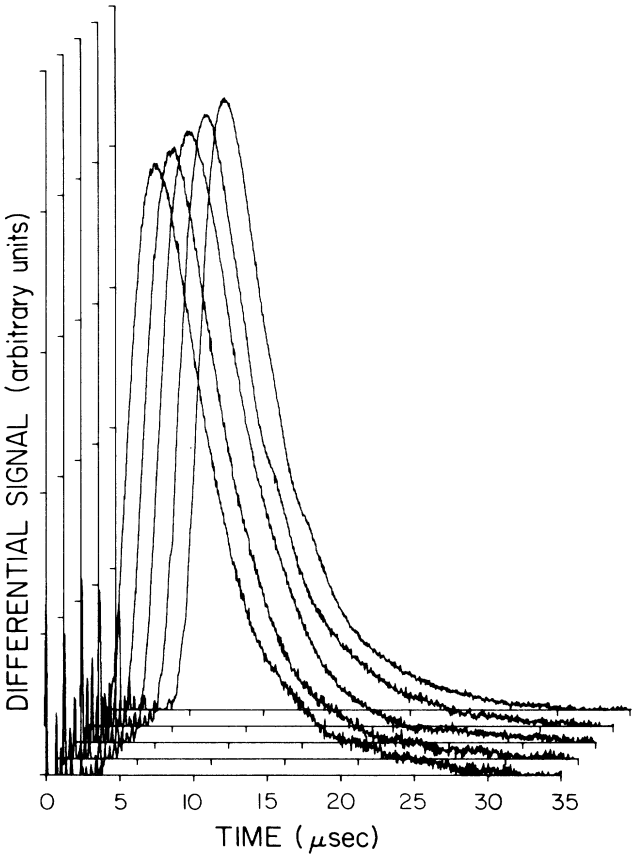

FIG. 12. $\partial S(t;t_p)/\partial t_p$ vs $t-t_p$ via finite differences for $T_s=2.88$ K. Front to back: $t_p=0.15$, 0.25, 0.35, 0.70, and 0.90 μsec; $\Delta t_p=0.10$, 0.10, 0.15, 0.20, and 0.30 μsec, respectively.

The global time constant, $\tau_{\exp}$, is constructed from the data of Fig. 10, as it is constructed from the model of Sec. III, by extrapolating the initial linear $\Delta n(t)$ to the point where it intercepts the saturation value of Δn. For the case discussed above, $T_s=3.46$ K, we find $\tau_{\exp}=1.1$ μsec. Values for the entire data set have already been shown in Fig. 6, where we saw that they are in good agreement both with the model, and with previous experiments. Uncertainties due to the saturation problem mentioned above, and in determining the initial desorption rate, are shown by the error bars in the figure.

An alternative method of analyzing the data is possible for pulses short compared to the time to reach saturation. Differentiating Eq. (20),

$$\frac{\partial S(t;t_p)}{\partial t_p}=\dot{n}(t_p)\int_{A_s} d^2r'\,S_0(\mathbf{r}-\mathbf{r}',\,t-t_p,\beta_s)\ . \tag{28}$$

Thus, by comparing $S(t)$ curves for pulses of width t_p and $t_p+\Delta t_p$, one obtains the instantaneous desorption rate at t_p, multiplied by the propagator referenced to time t_p. An example is shown in Fig. 12, where we have plotted $\Delta S(t)/\Delta t_p$ versus $t-t_p$, from $t_p=0.15$ to 0.90 μsec, for the data at $T_s=2.88$ K. When the curves are normalized to the same maximum value, to facilitate visual comparison, they become largely indistinguishable, qualitatively confirming that the propagator, $S_0(t-t_p)$, is basically the same in all of these cases. This observation is consistent with our assumption that the desorption proceeds isothermally [ideally, to account more properly for the fact that $\Delta n(\Delta t_p)$, the change in amount desorbed between t_p and $t_p+\Delta t_p$, actually varies in this sequence, the curves should be normalized to the same area].

We turn our attention next to experiments in which the pulse repetition time, t_r, is varied and all other parameters are fixed. An example is shown in Fig. 13, where $\nu_r=1/t_r$. Here, t_p was 50 μsec, long enough to reach steady state at $T_s=2.88$ K (the pulse width can be seen as an offset in the signal during the pulse-on period, probably caused by the effect on the bolometer of the magnetic field due to the current in the heater). As t_r is increased from 1 to 14 msec, the signal increases and finally saturates. The reason is that the longer t_r, the more the film readsorbs between pulses, until t_r is long enough to allow the film to regain its equilibrium coverage.

In Fig. 14 we plot the integrated signals, $\int S(t)dt$ versus t_r, for the data of Fig. 13, and for another set of experiments with $t_p=4$ μsec and $T_s=4.04$ K. Notice that both sets of data saturate at t_r well below $t_{rc}\simeq 14$ msec, where t_{rc} is the recovery time for pulses hot

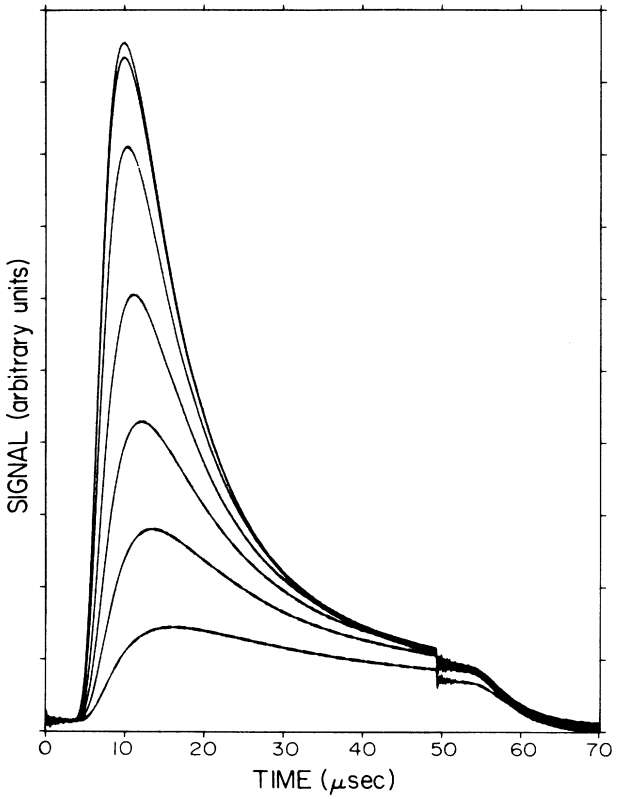

FIG. 13. $S(t)$ vs t, as a function of ν_r, for $T_s=2.88$ K and $t_p=50$ μsec. In descending order, $\nu_r=70$, 190, 270, 350, 450, 600, and 1000 Hz. Same vertical scale as in Fig. 8.

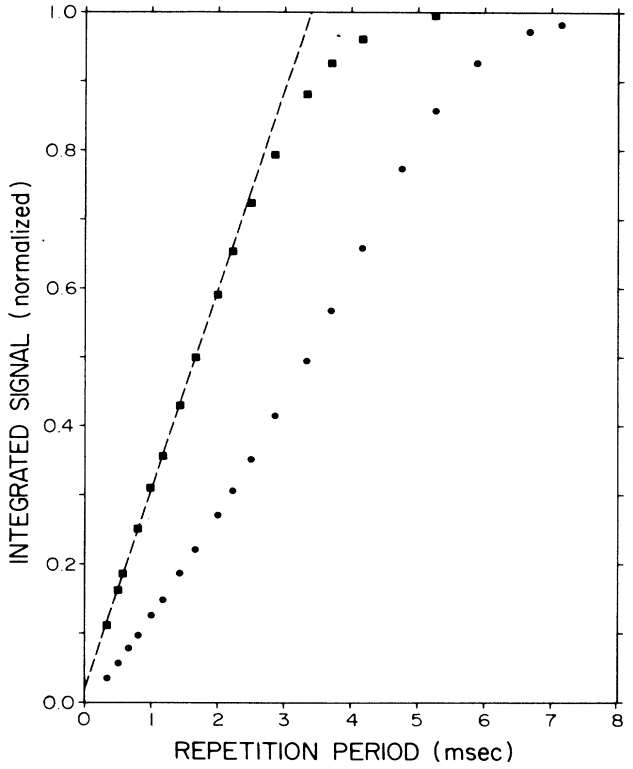

FIG. 14. $\int_0^{t_I} dt\, S(t)$ vs t_r, normalized to $\int_0^{t_I} dt\, S(t)$ at t_{rc}, for $T_s=2.88$ K, $t_p=50$ μsec (squares), and $T_s=4.04$ K, $t_p=4$ μsec (circles).

enough to desorb essentially the entire film.

The slope of each curve in the figure should be proportional to the net rate of adsorption, which we expect is given by

$$-\dot{n}(t)=\frac{\sigma}{\sqrt{2\pi m k_B T_0}}[P_f(T_0,n)-P_f(T_0,n_0)]\ . \quad (29)$$

This arises from Eq. (2) with all temperatures set equal to T_0 on the millisecond time scale of these experiments. Equation (29) makes it clear that the shape of these curves is governed by the adsorption isotherm at T_0. For example, if Henry's law ($P_f \propto n$) obtained, the curve would be a pure exponential. The data at $T_s=2.88$ K, in which $\dot{n}(t)$ appears constant until close to saturation, are of the form to be expected if $(\partial^2 P_f/\partial n^2)_{T_0}>0$, so that $P_f(T_0,n)\ll P_f(T_0,n_0)$ until almost the end of the recovery period.

The data at $T_s=4.04$ K, however, have an "S" shape, with a slope that increases before bending over near saturation. According to Eq. (29), however, $\dot{n}(t)$ should never increase with t since $(\partial P_f/\partial n)_T \geq 0$ is a thermodynamic stability condition for any adsorption system. A possible explanation of the anomaly might be that our assumption of constant sticking coefficient, σ, is violated, but there is a simpler and more convincing explanation: the behavior is due to the forward focusing effect of collisions among desorbing gas atoms.[9] The idea is that at small t_r, where relatively few atoms adsorb and desorb with each pulse, the linear region is collisionless. However, at $t_r \gtrsim 3$ msec, there is enough desorption in each pulse for collisions to begin to affect the data.

This conclusion is supported by an independent analysis of the integrated signal for long t_r at $T_s=4.04$ K. Assuming $\sigma=1$, using our independent calibration of the bolometer sensitivity, and evaluating the geometric integral over d^2r' in Eq. (26), we find a lower limit of 2.1 ML desorbed to produce a signal of the size observed. However, we have already placed an upper limit of 1.2 ML on the amount adsorbed. The discrepancy can only be reasonably reconciled by appealing to the forward focusing effect of collisions on the desorbing atoms.

These arguments suggest that data of the kind shown in Fig. 14 are an effective test of nearly collisionless desorption. The criterion is $\partial\dot{n}/\partial t_r \leq 0$, i.e., that the curve in Fig. 14 never be concave upward. Although the data at $T_s=4.04$ K (the highest-power pulses in our experiments) do not pass this test, the data at $T_s=2.88$ K and below all do so. These are also the data that are in best agreement with the phenomenological model, as discussed in Sec. III.

There are several other interesting and consistent features of these experiments which have a direct bearing on substantiating our theme that the desorption dy-

namics of these films is dominated by the nonlinearity of the underlying equilibrium adsorption isotherm and, in particular, the sign of its curvature.

Let us begin by comparing Fig. 8 to Fig. 13. In the first case, where t_r is held constant at its saturation value while t_p is varied, all the signals share the same rise, but differ at longer times. In the second case, where t_p is held at its saturation value and t_r varied, the signals rise along different curves, but share the same long-time behavior. The reason for this observation can be understood from Eq. (20) by referring to Fig. 15.

In the figure, the path followed by each of the two types of experiments is traced. The solid line illustrates what happens when the heater is turned on, while the dashed line shows what occurs when it is subsequently turned off. In those experiments where t_p is varied at constant saturation t_r, each cycle starts from the equilibrium point, (n_0, T_0), and changes the endpoint of desorption (n_1, T_s) by changing t_p. The common initial desorption rate accounts for the initial rise shared by all of the signals in this sequence since it originates from the first atoms to reach the detector. On the other hand, the tails differ because extending t_p changes both the integral in Eq. (20) as well as the desorption rate near the cycle endpoint. By contrast, when t_r is varied at constant saturation t_p, each signal is due to a cycle in which desorption ends at the same steady-state condition (n_{ss}, T_s), but begins at a different initial condition, (n_2, T_0), depending on t_r. This difference in initial conditions is clearly reflected in a different rise in the signal, but how do we understand the common tails? Since t_p is

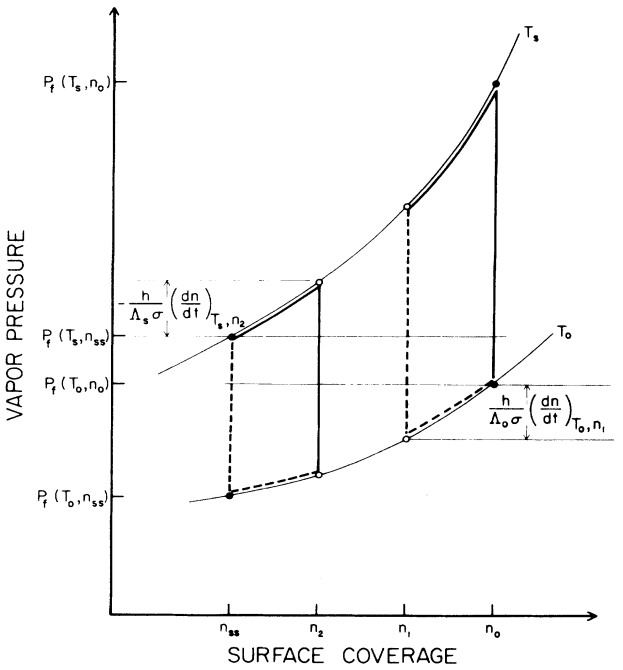

FIG. 15. Desorption at temperature T_s and readsorption at temperature T_0 illustrated schematically for different experiments over a positive-curvature segment of the vapor-pressure isotherms. Refer to text for discussion.

the same for all of the curves in this sequence, we might have expected each one to be identical in shape to the others when properly scaled to reflect the relative amounts desorbed. This is what we would predict from Eq. (20) if the desorption were exponential in time with a single time constant, but for a realistic isotherm we know that is not the case. How does this distinction affect the signal shapes we observe?

Suppose, as an example, we compare the signals for two different repetition periods—the t_r which brings us back to n_2 from steady state versus t_{rc}, the critical repetition period, which ensures our return to n_0. To do this we first linearly scale the trajectory from n_2 to n_{ss} so that it gives the same Δn as the trajectory from n_0 to n_{ss}, and the two signals then have the same area. This scaling can be visualized as stretching the distance from n_2 to n_{ss} along the horizontal line at $P_f(T_s,n_{ss})$ until it equals the distance from n_0 to n_{ss} while at the same time stretching the corresponding segment of the T_s isotherm; the two trajectories can now be compared directly. Because of the positive curvature of the isotherm illustrated, the actual vapor pressure at n_0, $P_f(T_s,n_0)$, exceeds the scaled value,

$$[(n_0-n_{ss})/(n_2-n_{ss})]P_f(T_s,n_2)\ .$$

As a consequence, the initial desorption rate [i.e., the distance to the line at $P_f(T_s,n_{ss})$] in the t_{rc} experiment exceeds that of the scaled t_r experiment. Because the two experiments give the same Δn, however, at some point in *time* the desorption rate along the t_{rc} trajectory must dip below that of the scaled t_r trajectory (even though this never happens as a function of coverage) since Δn is just the area under the $\dot{n}(t')$-versus-t' curve out to t_p. Therefore, if the isotherm has the structure illustrated, the relative weighting of desorption events favors earlier times relative to later ones with increasing repetition period; were the curvature to be reversed, we would find exactly the opposite result. Put another way, our observation that the signals in fact favor relatively later desorption events with decreasing t_r confirms with the predictions for an isotherm with positive curvature. That this effect is as pronounced as it is in the data is an indication of how strong this nonlinearity in the isotherm may indeed be. A parallel discussion of the desorption rates for a linear isotherm (which produces a simple exponential time dependence) would reveal a signal shape independent of t_r because the segments from n_2 to n_{ss} and from n_0 to n_{ss} form corresponding sides of similar triangles and the scaling procedure then makes the trajectories overlap identically.

We have also made observations in which either t_r or t_p is held fixed, below its saturation value, while the other is varied. For example, the behavior of the time-of-flight spectrum as a function of pulse width at a repetition interval well below t_{rc} is illustrated in Fig. 16. The substrate temperature, vertical scale, and the pulse-width sequence are identical with those in Fig. 8, so there is a one-to-one correspondence between the waveforms of each figure: the only difference is that the repetition rate has been changed from 70 to 1000 Hz. Sweeping through t_p, the amplitude of the signal at first increases

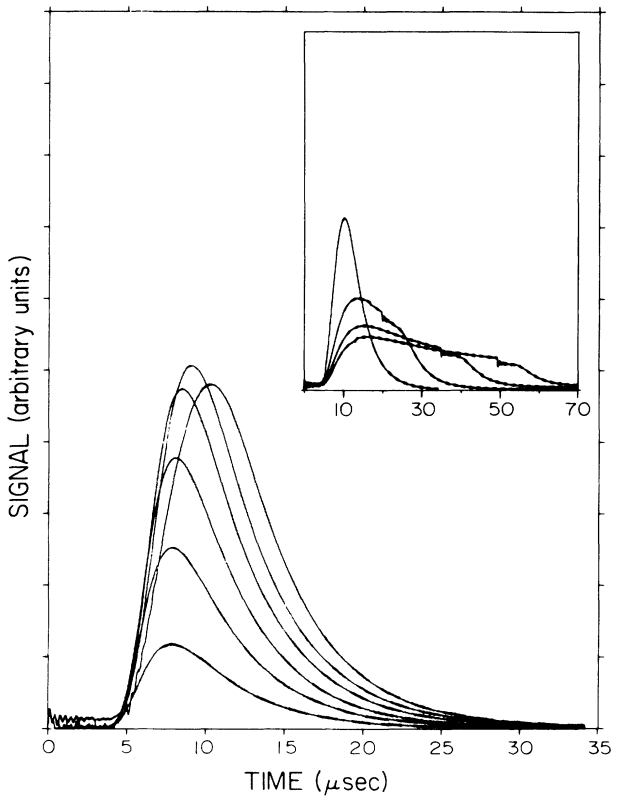

FIG. 16. $S(t)$ vs t, as a function of t_p, for $T_s=2.88$ K, $\nu_r=1000$ Hz. Main figure: left to right, $t_p=0.35$, 0.70, 1.2, 2.0, 3.0, and 5.0 μsec. Inset: $t_p=5.0$, 20, 35, and 50 μsec. Same vertical scale as in Fig. 8.

as previously, though at a noticeably slower rate; it then abruptly reaches a maximum but, unlike before, decreases with even longer pulse widths after that. The effect, while at first both curious and surprising, can also be understood in terms of Fig. 15.

The key is to recognize that the actual closed path followed by the system is determined by a self-consistency condition, imposed by the periodicity of the experiment, that requires the number desorbed in each pulse to be equal to the number that can be adsorbed before the next one. Thus, while the amplitudes and shapes of the time-of-flight signals illustrated in Fig. 16 exhibit unusual features, the sequence of areas, and therefore the number desorbed, follows a simple and uniform behavior, growing steadily with t_p until reaching a maximum value proportional to the amount which can be reaccumulated in the film during t_r. Referring to Fig. 15, suppose that $n_0-n_1=\Delta n(t_{p_1})$ is also equal to $\Delta n(t_r)$, the maximum number which can be readsorbed between pulses. This is emphasized in the figure by the fact that n_0, n_1, n_2, and n_{ss} are labeled in a way marking off equal Δn increments between them. We then reason crudely as follows. For $t_p \leq t_{p_1}$ we always trace out cycles starting at n_0 because the film is capable of reaccumulating a Δn equal to the amount desorbed in the repetition time allotted. When t_p exceeds t_{p_1}, however, the maximum amount which can be desorbed must be limited by $\Delta n(t_r)$; since the total desorption time has increased, the only way the system can still desorb the same amount as previously is for it to do so at an overall slower rate. This means beginning from a reduced vapor pressure (i.e, sliding down the isotherm) so that, for example, we execute a cycle between n_1 and n_2 maintaining the same Δn. With t_p large enough, the system finally ends up cycling between n_2 and n_{ss}. More generally, if t_r is insufficient to guarantee the film always returns to equilibrium, or if t_p is not long enough to ensure that the film is always driven arbitrarily near steady state, then we will probe a succession of intermediate cycles in the figure whose starting and ending point will depend on both t_p and t_r.

The decrease in signal amplitude we observe in Fig. 16 therefore has a natural explanation. Its onset marks our emergence from pulse-width–constrained desorption into the regime of repetition-rate–constrained desorption where the signal area remains fixed. The amplitude of these wave forms must consequently decrease as they become broader in order to preserve their area and keep the number of atoms desorbed constant. For very short pulse widths, the signal versus time is identical with that in the time-constant experiment (compare Fig. 8), whereas for long pulses it looks just like the waveforms in the repetition-rate experiment (compare Fig. 13). A linear equation of state demands an interesting prediction in this regard which runs counter to the actual behavior of the data. Were this to be the case, then each waveform in Fig. 16 would be a miniature of the corresponding one in Fig. 8 with a scale factor that depended on the pulse width (and, of course, approached 1 as t_p went to zero). This assertion follows from the self-similarity property of the exponential functions which are solutions of the linear equations of motion. That is, except for a scaling factor, equal-width segments of the $n(t)$-versus-t curve are identical and, as a consequence, the net desorption rate as a function of time looks the same independent of one's starting point; it is only this initial condition which varies with t_r for fixed t_p. As we have already pointed out in our discussion of Fig. 13, however, aside from the decrease in amplitude resulting from the need to preserve area, any further discrepancies between the waveforms of Figs. 16 and 8 must be attributed to a substantial nonlinearity in the isotherm.

V. CONCLUSIONS

We believe we have succeeded in this paper in showing that many quantitative and qualitative features of our flash desorption experiments can be plausibly accounted for on the basis of phenomenological arguments and the equilibrium thermodynamic properties of adsorbed films. In particular, even though the kinetics of desorption obey highly nonlinear equations yielding no simple time constant, an overall time scale for reaching steady state can be extracted from our model by a relatively simple procedure. When this prediction is compared with experiment, very good agreement is found, especially under conditions where collisions between desorbing atoms become unimportant. The central

physical picture that emerges is that when the substrate of a film in equilibrium, and with a low vapor pressure, is suddenly heated, the film temperature jumps rapidly to that of the substrate, and it subsequently desorbs at a rate that is governed by its vapor pressure and the curvature of its adsorption isotherm.

A major lesson of this analysis is that a great deal of information regarding the behavior of these films may be deduced from phenomenological reasoning. The role of more sophisticated, microscopic theories then becomes to predict those quantities that are the starting points of these arguments: equilibrium isotherms and sticking coefficients. The former is a standard problem of many-body theory. The latter, calculation of the sticking coefficient, is the key theoretical problem in desorption kinetics.

We have assumed throughout a constant sticking coefficient equal to 1. That assumption is consistent with the spirit of our model, and there is experimental evidence that it is of that order of magnitude in the system we have studied.[8] However, there is also evidence that it may be significantly smaller on other surfaces.[33]

We would hope, then, that one consequence of our work would be to re-emphasize the importance of finding the sticking coefficient, both theoretically and experimentally. The theoretical task is to relate the sticking coefficient to fundamental properties such as the time-dependent adsorption potential. The experimental challenge is to measure the sticking coefficient, as a function of parameters such as film coverage and incident energy and angle, particularly on surfaces that are—unlike the ones we have used—well characterized by techniques such as Auger spectroscopy and electron diffraction.

In spite of these remaining unsolved problems, however, one should not lose sight of the striking success we have demonstrated in bringing theory and experiment to the point where they can be reasonably compared. That success justifies the fundamental assumption of quasiequilibrium desorption, and opens the way for more detailed experiments to be compared with more precise theories in the future.

ACKNOWLEDGMENTS

This work was supported by U.S. Office of Naval Research (ONR) Contract No. N00014-80-C-0447 and U.S. Department of Energy (DOE) Contract No. DE-FG03-85ER45192. One of us (M.W.) especially wishes to thank Dr. G. John Dick, of the California Institute of Technology Low Temperature Physics Laboratory, for several timely and illuminating discussions. The technical assistance of Mr. Edward Boud is also gratefully acknowledged.

---

*On leave from the Rockwell International Science Center, Thousand Oaks, CA 91360.

[1]H. J. Kreuzer and Z. W. Gortel, *Physisorption Kinetics* (Springer-Verlag, New York, 1986).
[2]G. Comsa and R. David, Surf. Sci. Rep. **5**, 145 (1985).
[3]G. Comsa, in *Dynamics of Gas Surface Interaction,* edited by G. Benedek and V. Valbusa (Springer-Verlag, New York, 1982), p. 117.
[4]M. J. Cardillo, M. Balooch, and R. E. Stickney, Surf. Sci. **50**, 263 (1975).
[5]M. Weimer and D. Goodstein, Phys. Rev. Lett. **50**, 193 (1983).
[6]M. J. Cardillo and J. C. Tully, in *Dynamics on Surfaces,* edited by B. Pullman *et al.* (Reidel, Dordrecht, 1984), p. 169.
[7]M. Sinvani, P. Taborek, and D. Goodstein, Phys. Rev. Lett. **48**, 1259 (1982).
[8]M. Sinvani, M. W. Cole, and D. L. Goodstein, Phys. Rev. Lett. **51**, 188 (1983).
[9]D. L. Goodstein, R. Maboudian, F. Scaramuzzi, M. Sinvani, and G. Vidali, Phys. Rev. Lett. **54**, 2034 (1985)
[10]D. Goodstein, and M. Weimer, Surf. Sci. **125**, 227 (1983).
[11]F. O. Goodman, Surf. Sci. **24**, 667 (1971).
[12]B. Bendow and S. C. Ying, Phys. Rev. B **7**, 622 (1973).
[13]S. C. Ying and B. Bendow, Phys. Rev. B **7**, 637 (1973).
[14]F. O. Goodman and I. Romero, J. Chem. Phys. **69**, 1086 (1978).
[15]Z. W. Gortel, H. J. Kreuzer, and D. Spaner, J. Chem. Phys. **72**, 234 (1980).
[16]Z. W. Gortel, H. J. Kreuzer, and R. Teshima, Phys. Rev. B **22**, 5655 (1980).
[17]Z. W. Gortel, H. J. Kreuzer, and R. Teshima, Phys. Rev. B **22**, 512 (1980).
[18]P. Summerside, E. Sommer, R. Teshima, and H. J. Kreuzer, Phys. Rev. B **25**, 6235 (1981).
[19]F. O. Goodman, Surf. Sci. **120**, 251 (1982).
[20]E. Sommer and H. J. Kreuzer, Phys. Rev. Lett. **49**, 61 (1982). This reference treats adatom interactions in a mean-field approximation.
[21]C. Jedrzejk, K. F. Freed, S. Efrima, and H. Metiu, Chem. Phys. Lett. **79**, 227 (1981).
[22]D. O. Edwards, P. Fatouros, G. G. Ihas, P. Mrozinski, S. Y. Shen, F. M. Gaspirini, and C. P. Tam, Phys. Rev. Lett. **34**, 1153 (1975).
[23]M. Weimer, Ph.D. thesis, California Institute of Technology, 1986.
[24]B. Axan, B.sc. thesis, California Institute of Technology, 1984.
[25]Y. S. Touloukian and E. H. Buyco, *Thermophysical Properties of Matter* (Plenum, New York, 1970), Vol. 4.
[26]O. Weis, Z. Angew. Phys. **26**, 325 (1969).
[27]P. Herth and O. Weiss, Z. Angew. Phys. **29**, 101 (1969).
[28]A. B. Williams, *Electronic Filter Design Handbook* (McGraw-Hill, New York, 1981).
[29]M. Sinvani and D. Goodstein, Surf. Sci. **125**, 291 (1983).
[30]J. P. Cowin, D. J. Auerbach, C. Becker, and L. Wharton, Surf. Sci. **78**, 545 (1978).
[31]J. P. Cowin, Phys. Rev. Lett. **54**, 368 (1985).
[32]M. W. Cole (private communication).
[33]P. Taborek and L. J. Senator, Phys. Rev. Lett. **56**, 628 (1986).